

Figure 1. A: baseline electrocardiogram with first-degree AVB and right bundle branch block and left axis deviation. B: LBBP; typical rsr' morphology with normal axis. C: typical "W" morphology in V1 before lead penetration of IVS. D: initial penetration of the IVS with shortening of the paced QRS interval (212 ms) and of the LVAT interval (162 ms). E: capture of the left bundle with rsr' morphology in V1, narrower QRS interval (148 ms) and shorter LVAT (108 ms). AVB, atrioventricular block; IVS, interventricular septum; LBBP, left bundle branch pacing; LVAT, left ventricular activation time. gr1.

AUTHORS' CONTRIBUTIONS

F.J. Bermúdez-Jiménez collected and analyzed the data; he wrote the manuscript with the help of the other authors. M. Molina-Lerma and P. Sánchez-Millán performed and supervised the technical procedures. J. Jiménez-Jáimez and R. Macías-Ruiz conceived the idea presented. M. Álvarez supervised the overall process. All authors discussed the results and contributed to the final manuscript.

CONFLICTS OF INTEREST

The authors have nothing to declare.

Francisco José Bermúdez-Jiménez,^{a,b,c,*} Manuel Molina-Lerma,^{a,b} Rosa Macías-Ruiz,^{a,b} Pablo Sánchez-Millán,^{a,b} Juan Jiménez-Jáimez,^{a,b} and Miguel Álvarez^{a,b}

^aServicio de Cardiología, Hospital Universitario Virgen de las Nieves, Granada, Spain

^bInstituto de Investigación Biosanitaria ibs.GRANADA, Granada, Spain

^cCentro Nacional de Investigaciones Cardiovasculares (CNIC), Madrid, Spain

* Corresponding author:

E-mail address: bermudezfrancisco23y@gmail.com

(F.J. Bermúdez-Jiménez).

Available online 9 October 2021

REFERENCES

- López-Sainz Áaue, Hernandez-Hernandez A, Gonzalez-Lopez E, et al. Clinical profile and outcome of cardiac amyloidosis in a Spanish referral center. *Rev Esp Cardiol.* 2021;74:149–158.
- González-López E, Gagliardi C, Dominguez F, et al. Clinical characteristics of wild-type transthyretin cardiac amyloidosis: disproving myths. *Eur Heart J.* 2017;38:1895–1904.
- Donnellan E, Wazni OM, Hanna M, Kanj M, Saliba WI, Jaber WA. Cardiac Resynchronization Therapy for Transthyretin Cardiac Amyloidosis. *J Am Heart Assoc.* 2020;9:e017335.
- Zanon F, Pastore G, Marcantoni L. Estimulación por marcapasos del haz de His: el mito se hace realidad. *Rev Esp Cardiol.* 2020;73:611–614.
- Wu S, Chen X, Wang S, et al. Evaluation of the criteria to distinguish left bundle branch pacing from left ventricular septal pacing. *JACC Clin Electrophysiol.* 2021. <http://doi.org/10.1016/j.jacep.2021.02.018>.

<https://doi.org/10.1016/j.rec.2021.08.016>

1885-5857/© 2021 Sociedad Española de Cardiología. Published by Elsevier España, S.L.U. All rights reserved.

Fluoroscopic-based algorithm for commissural alignment assessment after transcatheter aortic valve implantation



Método para la evaluación angiográfica del alineamiento comisural tras el implante percutáneo de válvula aórtica

To the Editor,

Recently, different strategies have been described for achieving commissural alignment during transcatheter aortic valve implan-

tation (TAVI).^{1–3} Computed tomography (CT) is the most accurate imaging technique to measure final orientation after TAVI implant. However, post-TAVI CT is not performed routinely and not clinically justified. Other strategies like co-registry of pre-TAVI CT and fluoroscopy could be useful but are not the standard of care.¹ We propose an algorithm to identify the final position of TAVI devices with recognizable commissural markers relying only in fluoroscopy with a resolution of 15° degrees.

Using a CT derived aortic root simulation, different rotational orientations of a virtual TAVI device were tested, ranging from

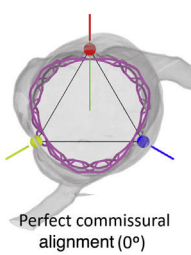
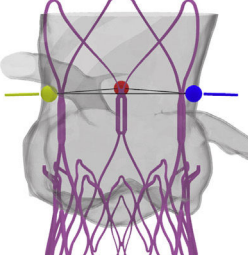
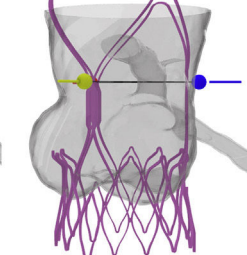
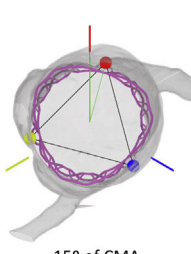
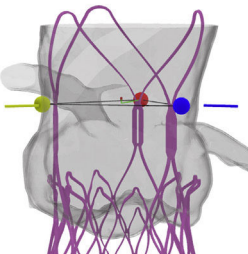
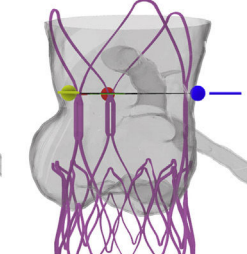
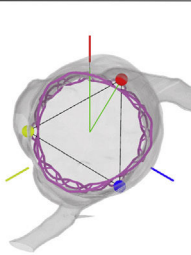
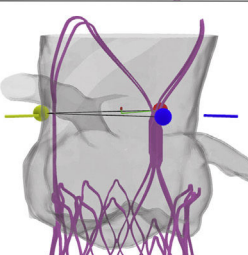
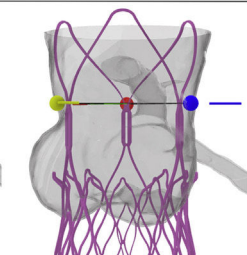
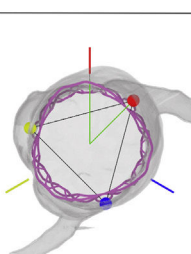
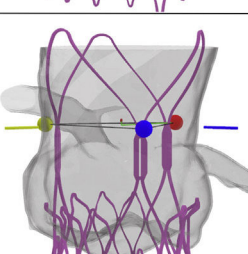
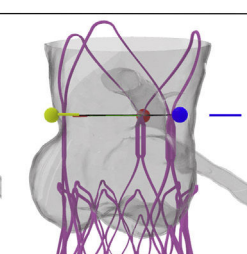
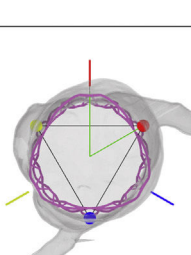
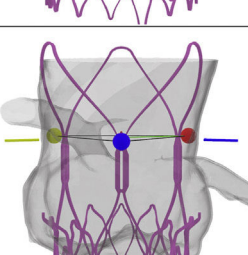
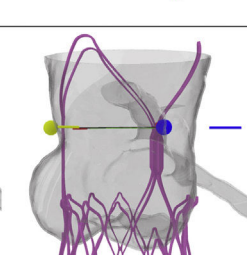
| Landmarks for CMA | 3-cusp view | 2-cusp view | Fluoroscopy tips | CMA classification |
|---|---|---|--|---|
|  <p>Perfect commissural alignment (0°)</p> |  |  | <p>Overlapping commissural markers at the outer curve of the aorta in 2-cusp view</p> | <p>COMMISSURAL ALIGNMENT 0°-15°</p> |
|  <p>15° of CMA</p> |  |  | <p>One commissural marker at the back (red) in 3-cusp view shifted to one side. Two commissural markers at the outer curve of the aorta in 2-cusp view</p> | <p>MILD CMA 15°-30°</p> |
|  <p>30° of CMA</p> |  |  | <p>Overlapping commissural markers in 3-cusp view. The 2-cusp view is not required</p> | <p>MODERATE CMA 30°-45°</p> |
|  <p>45° of CMA</p> |  |  | <p>Commissural marker at the front (blue) shifted to one side in 3-cusp view. In the 2-cusp view 2 markers are shifted to the inner curve of the aorta</p> | <p>SEVERE CMA >45°</p> |
|  <p>60° of CMA</p> |  |  | <p>Overlapping commissural markers at the inner curve of the aorta in 2-cusp view</p> | |

Figure 1. Landmarks for fluoroscopic identification of commissural alignment. CMA: commissural misalignment. Red line: left coronary to non-coronary native commissure. Blue line: left coronary to right coronary native commissure. Yellow line: right coronary to non-coronary native commissures. Colored circles highlight the commissural markers of the transcatheter aortic valve implantation device (colors match the lines of the native commissures in a commissural aligned implant). CMA, commissural misalignment.

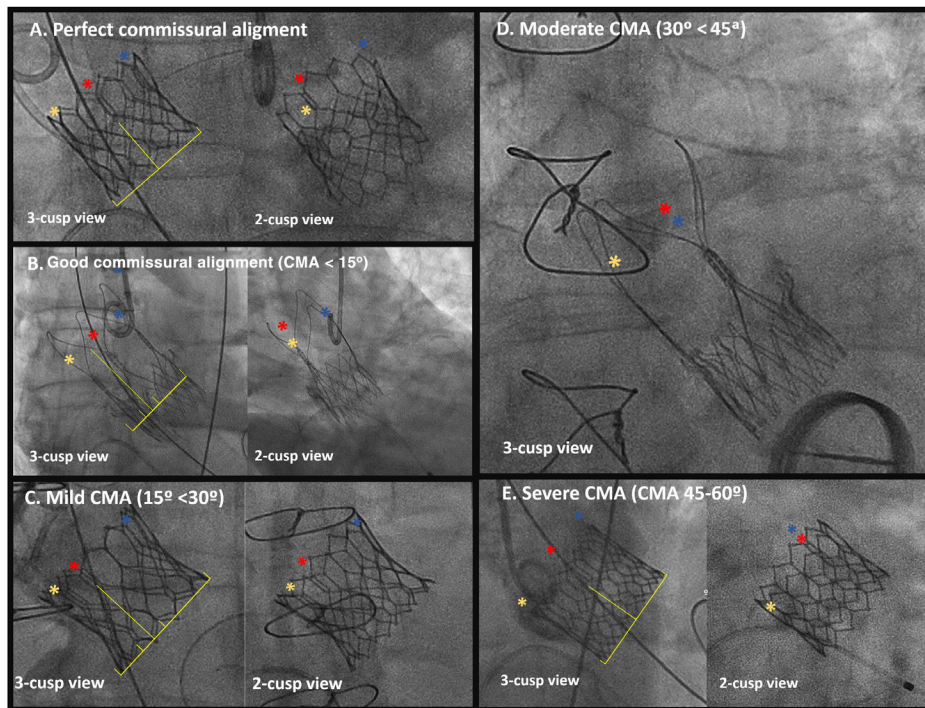


Figure 2. Examples of the application of the algorithm for commissural alignment assessment. A: perfect commissural alignment. One commissural marker is centered in 3-cusp view and 2 commissural markers are overlapped at the outer curve of the aorta in 2-cusp view. B: good commissural alignment ($< 15^\circ$). One commissural marker is shifted to one side within inner quarter of the radius of the valve stent frame with overlapped commissural markers at the outer curve of the aorta in 2-cusp view. C: mild commissural misalignment (15° – 30°). One commissural marker is shifted beyond the inner quarter in the 3-cusp view with two commissural markers located at the outer curve of the aorta in the 2-cusp view. D: moderate commissural misalignment (30° – 45°): commissural markers are overlapping at either side in the 3-cusp view. E: severe commissural misalignment (45° – 60°). One commissural marker is within the inner quarter of the stent frame radius in the 3-cusp view and 2 commissural markers are located at the inner curve of the aorta; in the worst scenario (a misalignment at 60°), one commissural marker is centered in the 3-cusp view with commissural markers overlapping at the inner curve of the aorta in 2-cusp view. CMA, commissural misalignment.

perfect commissural alignment to complete misalignment. The relationship between the commissural markers (CM) and the native commissures was evaluated in a simulated 3-cusp and 2-cusp (right coronary cusp to left coronary cusp) views. From the results obtained, we can determine the degree of commissural misalignment (CMA) as follows (figure 1, video 1 of the supplementary data):

1. Perfect commissural alignment (0°): in the 3-cusp view one commissural marker is centered back. In the 2-cusp view, 2 commissural markers are overlapping each other at the outer curve of the aorta.
2. 15-degree CMA (15°): the CM located at the back of the aorta is shifted to one side, intersecting the inner quarter radius of the stent frame in the 3-cusp view. In the 2-cusp view, 2 CM are close to the outer curve of the aorta.
3. 30-degree CMA (30°): in the 3-cusp view 2 CM are overlapping, either at the inner or at the outer curve of the aorta, depending on the direction of the misalignment. The 2-cusp view is not needed in this orientation.
4. 45-degree CMA (45°): in the 3-cusp view one CM is shifted to one side of the center of the aorta, intersecting the inner quarter of stent frame radius. Conversely to the 15° position, in the 2-cusp view two CM appear close to the inner curve of the aorta.
5. 60-degree CMA (60°): in the 3-cusp view the image is similar to the “perfect commissural alignment”. However, in this case one CM is centered front. In the 2-cusp view 2 CM appear overlapping at the inner curve of the aorta.

The proposed algorithm stratifies the orientation of TAVI using the current established classification for CMA¹: aligned (0° – 15°), mild CMA (15° – 30°), moderate CMA (30° – 45°) and severe CMA (45° – 60°).

The clinical applicability of this algorithm was tested in 18 patients. Twelve patients were included in an ongoing prospective study evaluating a method to achieve a commissural alignment implant,³ CT was used to measure the final implant orientation. Other 6 patients who received a conventional implant were included; in those cases, fluoroscopy, and CT co-registry¹ were used to evaluate the implant orientation. Patients provided informed consent and the study was approved by the ethical committee of the center. One cardiologist, blinded to the results, was trained in the proposed algorithm; 16/18 patients were correctly assigned to their CMA group, only 2 cases with a CMA near 15° were misclassified as good commissural alignment while CT scan reveal mild CMA.

There are some limitations of this method: a) TAVI devices without identifiable radiopaque markers for all 3 commissural posts (Evolut Medtronic, USA) cannot be evaluated although newer iteration will incorporate them; b) 2 complementary projections are needed to perform the analysis (3-cusp and 2-cups views), but there is no need for additional contrast dye administration.

Examples of actual cases with assessment of the degree of CMA using the aforementioned algorithm are shown in figure 2.

In conclusion, the degree of CMA of TAVI can be easily measured immediately after the implant based exclusively on fluoroscopy. CMA has not only investigational relevance, but also potential clinical benefits in patients requiring eventual coronary angiograms or valve-in-valve procedures and might be associated to

better residual gradients, lower pacemaker rate, and reduced risk of leaflet thrombosis.

FUNDING

This investigation received funding resources from the Spanish Society of Cardiology (SEC) with the grant number: SEC/FEC-INV-CLI 21/023. Alfredo Redondo Diéguez is beneficiary of a *Contrato Rio Hortega* grant from the *Instituto de Salud Carlos III*: CM20/00068. The project was developed thank to a FIS grant (PI21/01188, from the *Instituto de Salud Carlos III, Madrid, Spain*).

AUTHORS' CONTRIBUTIONS

A. Redondo designed the project and, in collaboration with I.J. Amat-Santos and S. Santos-Martínez, wrote the final manuscript. R. Delgado-Arana, C. Baladrón Zorita and J.A. San Roman performed a critical review and approved the final version of the manuscript

CONFLICTS OF INTEREST

I.J. Amat-Santos is proctor for Boston Scientific, Meril Life and Medtronic. There are no other conflicts of interest to declare.

APPENDIX. SUPPLEMENTARY DATA

Supplementary data associated with this article can be found in the online version available at <https://doi.org/10.1016/j.rec.2021.08.010>

Alfredo Redondo,^{a,b,*} Sandra Santos-Martínez,^{a,b}

Raúl Delgado-Arana,^{a,b} Carlos Baladrón Zorita,^{a,b}
J. Alberto San Román,^{a,b} and Ignacio J. Amat-Santos^{a,b}

^a*Departamento de Cardiología, Hospital Clínico Universitario, Valladolid, Spain*

^b*Centro de Investigación Biomédica en Red de Enfermedades Cardiovasculares (CIBERCV), Spain*

* Corresponding author:

E-mail address: alfredoredondo@gmail.com (A. Redondo).

Available online 9 October 2021

REFERENCES

1. Tang GHL, Zaid S, Fuchs A, et al. Alignment of Transcatheter Aortic-Valve Neo-Commissures (ALIGN TAVR): Impact on Final Valve Orientation and Coronary Artery Overlap. *JACC Cardiovasc Interv.* 2020;13:1030–1042.
2. Takamatsu M, Fuku Y, Ohya M, Shimamoto T, Komiya T, Kadota K. Lateral Approach for Modifying Hat-Marker Orientation to Minimize Neo-Commissural Overlap During Transcatheter Aortic Valve Replacement. *JACC Cardiovasc Interv.* 2020;13:e199–e201.
3. Redondo A, Valencia-Serrano F, Santos-Martínez S, et al. Accurate commissural alignment during ACURATE neo TAVI procedure. *Proof of concept Rev Esp Cardiol.* 2021. <http://doi.org/10.1016/j.rec.2021.02.004>.

<https://doi.org/10.1016/j.rec.2021.08.010>

1885-5857/ © 2021 Sociedad Española de Cardiología. Published by Elsevier España, S.L.U. All rights reserved.

Brugada phenocopy in a child with pediatric inflammatory multisystemic syndrome caused by SARS-CoV-2



Fenocopia de Brugada en el contexto de síndrome inflamatorio multisistémico pediátrico asociado con el SARS-CoV-2

To the Editor,

Brugada syndrome (BS) is an inherited channelopathy associated with elevated risk of ventricular fibrillation and sudden cardiac death. Its diagnosis is based on a standard electrocardiographic pattern comprising ST-segment elevation ≥ 2 mm in right precordial leads (V_1 and V_2), followed by a negative T wave (type 1 Brugada pattern). This pattern can be spontaneously observed or induced by fever or a provocation test involving sodium channel blockers. However, certain drugs and conditions (eg, electrolyte imbalances, myocardial ischemia) can induce type 1 Brugada pattern in individuals without the congenital syndrome.¹ Riera et al.² named this condition “Brugada phenocopy” (BrP) when it meets a series of diagnostic criteria³: an electrocardiographic pattern compatible with types 1 or 2 Brugada, a plausible cause, normalization of the electrocardiographic pattern after its resolution, low probability of BS, absence of compatible symptoms and personal and family history, a negative genetic study, and a negative provocation test with sodium channel blockers.

In May 2020, reports began to appear of children who developed, weeks after acute SARS-CoV-2 infection, a multisystem

inflammatory syndrome of variable expressivity that was named pediatric multisystem inflammatory syndrome related to SARS-CoV-2 (SIM-PedS).⁴ These symptoms can present as complete or incomplete Kawasaki disease and in conjunction with gastrointestinal symptoms, shock, hypotension, and myocardial dysfunction.

The cardiac involvement of SARS-CoV-2 can include electrocardiographic changes compatible with BrP. However, no “confirmed” phenocopy has been described in this context.

We present the case of a 12-year-old boy admitted with a 4-day history of abdominal pain, diarrhea, vomiting, and 40 °C fever. At admission, he had blood pressure of 74/41 mmHg (< 5th percentile for his age and weight), tachycardia, and normal oxygen saturation. His overall condition was poor on examination, with cracked lips, conjunctival hyperemia, and strawberry tongue. Blood tests showed elevations in inflammatory markers (C-reactive protein, 32 mg/dL), with NT-proBNP at 14 700 pg/mL and troponin I at 1581 ng/L. Serological tests were positive for immunoglobulin G for SARS-CoV-2. The patient met clinical and analytical criteria compatible with SIM-PedS.

Electrocardiography (figure 1A) revealed type 1 Brugada pattern. Echocardiography showed a left ventricular ejection fraction of 55%, with no other abnormalities.

Given his poor hemodynamic improvement, with blood pressure consistently less than the 5th percentile for his age, he was admitted to the pediatric intensive care unit for vasoactive support. In addition, treatment against SIM-PedS was administered, comprising intravenous immunoglobulin, aspirin, and methylprednisolone, which improved the clinical situation